Photoemission study of the valence-band electronic structure in Fe_xO, Fe_3O_4, and α-Fe_2O_3 single crystals

Robert J. Lad* and Victor E. Henrich
Applied Physics, Yale University, P.O. Box 2157, New Haven, Connecticut 06520
(Received 8 August 1988)

Valence-band photoemission spectra have been measured from cleaved stoichiometric iron oxide single crystals using synchrotron radiation. The total photoelectron yield is observed to increase dramatically at photon energies above the Fe $3p \rightarrow 3d$ excitation threshold, and the resonant onset correlates directly with the oxidation state of the Fe cations. Features in the total yield profiles are interpreted in terms of atomic multiplets. The phenomenon of resonant photoemission is used to distinguish the Fe $3d$-derived valence states from the overlapping unhybridized O $2p$ states in each of the oxides. By use of cleaved single crystals, the subtle differences in the valence-band photoemission features associated with ferrous (Fe^{2+}) and ferric (Fe^{3+}) cations have been determined. The measured energy distribution of the photoemission final states in single crystal α-Fe_2O_3 are in good agreement with recent measurements and configuration-interaction cluster calculations by Fujimori *et al.*, which take into account ligand-to-metal charge transfer. Constant-initial-state spectra measured across the $3p \rightarrow 3d$ threshold in each oxide indicate that most of the photoemission intensity near the top of the valence band is derived from hybridized cation-$3d$–ligand-$2p$ states, whereas the emission at higher binding energies results from primarily $3d^{n-1}$ final states. On this basis, each of the iron oxides is classified as a charge-transfer rather than a Mott-Hubbard insulator.

I. INTRODUCTION

The interpretation of the valence-band photoemission spectra from iron oxides has been a long-standing challenge in surface science and has been the subject of many experimental[1–11] and theoretical[12–18] studies. Despite extensive investigation, an understanding of the electronic structure of these and other transition-metal oxides is not yet complete. The difficulty in interpreting their photoemission spectra arises from the complexity of multielectron correlation effects and from the hybridization between cation and anion valence states.

Early analyses of the valence-band photoemission spectra from iron oxides were based on the assumption of localized $3d$ cation levels in a ligand field, and the photoemission features were correlated to the calculated multiplet and crystal-field-split final states.[1,4] Better agreement with experiment was attained by including configuration interactions (CI) within the $3d$ manifold and allowing for covalency effects.[6,12,13] Fujimori *et al.*[2,6] have recently reported resonant photoemission measurements from sintered nonstoichiometric Fe_xO and α-Fe_2O_3 samples that were scraped with a diamond file in ultrahigh vacuum. Their results show that the Fe $3d$-derived features in the valence band extend to about 16 eV below the Fermi level in both compounds. A comparison of the experimental spectra with a CI calculation for a $(FeO_6)^{9-}$ cluster[6] suggests that the large valence-band width is due to the presence of both $3d^{n-1}$ and $3d^nL$ photoemission final states (where L represents a ligand hole), with the latter being associated with ligand-to-metal charge-transfer screening of the $3d$ holes created during photoemission. Zaanen *et al.*[17,18] have formulated the concept of ligand-to-metal charge transfer into a generalized theory for the electronic structure of transition-metal compounds that is based on an Anderson impurity approximation.

In this paper we report the results of resonant photoemission measurements of the valence band from cleaved Fe_xO, Fe_3O_4, and α-Fe_2O_3 single-crystal surfaces across the Fe $3p \rightarrow 3d$ photoabsorption threshold using synchrotron radiation. By using single crystals, the energy distribution of Fe $3d$ and O $2p$ states in the valence-band photoemission spectra is observed in samples with well-defined and uniform cation environments; this is in contrast to the multiple cation valence states usually found in the nonstoichiometric oxide films grown on metallic iron. We use the resonant photoemission phenomenon to identify the $3d$-derived states associated with the ferrous (Fe^{2+}) and ferric (Fe^{3+}) cations in each compound. Our results are consistent with Fujimori's charge-transfer interpretation of the valence-band photoemission spectra of Fe_xO and α-Fe_2O_3 and also indicate that similar charge-transfer mechanisms may exist in Fe_3O_4.

In Sec. II details are given concerning the sample characteristics and the measurement techniques. Section III presents results for the photoelectron yield at photon energies across the Fe $3p$ threshold for each of the iron oxides. In Secs. IV and V the resonant valence-band photoemission results are presented and discussed in relation to previously reported photoemission studies of iron oxides.

II. EXPERIMENT

Each of the iron oxide single crystals used in this study was grown and annealed under controlled oxygen partial pressures to yield uniform and nearly ideal stoichiometries; the Fe_xO crystal had a composition of $Fe_{0.945}O$, which is the highest Fe/O ratio attainable while remaining in the Fe_xO single-phase field.[19] Laue x-ray diffraction patterns were very sharp, indicative of excellent crystal quality. Cleavage samples were made by aligning and grooving the crystals along the precise crystallographic orientations which yielded the best fracture surfaces: (100) for Fe_xO, (110) for Fe_3O_4, and $(10\bar{1}2)$ for α-Fe_2O_3. A blade-and-anvil arrangement was used to cleave the samples *in situ* at pressures below 2×10^{-10} Torr. In general, the cleavage faces were not perfectly smooth after fracture, but they did contain large flat areas that were used for analysis.

The photoemission experiments were performed on beamline U14 at the National Synchrotron Light Source (NSLS) at Brookhaven National Laboratory. A plane grating monochromator provided photons over the energy range $30 \le h\nu \le 100$ eV, which were directed onto the samples at an angle of 45° with respect to the surface normal. Angle-integrated photoemission spectra were obtained with a Physical Electronics 15-255G double-pass cylindrical-mirror analyzer, operating at 25 eV pass energy. The energy resolution in the measured spectra was limited primarily by the monochromator; the resolution at $h\nu=50$ eV is approximately 0.3 eV. The energy distribution curves (EDC's) measured from each of the iron oxide samples are referenced to the Fermi level (E_F), as determined from a clean gold foil.

All of the photoemission data were normalized to the incident photon intensity through the use of a high-transmission Au-coated grid and electron multiplier flux monitor assembly[20] situated in the path of the beam. Total photoelectron yield (TY) measurements shown in Sec. III were measured simply by detecting the photoinduced current to the sample ground. An inelastic background subtraction procedure was used for some of the spectra presented in Sec. IV. The integral inelastic background at each point was assumed to be proportional to the total integrated intensity at higher kinetic energies. Constant-initial-state (CIS) spectra measured across the Fe 3*p* excitation threshold were obtained directly from the EDC's by plotting the intensity above the inelastic background at a given binding versus photon energy. No attempt was made to correct for the decreasing analyzer transmission with increasing kinetic energy of the photoelectrons since that effect is small compared to the resonant behavior of interest.

III. PHOTOELECTRON YIELD ACROSS THE 3*p* EXCITATION THRESHOLD

Recently there has been much interest in the resonant photoemission effects that are observed when the photon energy is tuned near the 3*p* excitation threshold in transition metals and their compounds.[21] Experiments on atomic Fe and other transition-metal vapors[22–24] have shown that excitations of the type $3p^63d^n \rightarrow [3p^53d^{n+1}]^*$ dominate at the 3*p* threshold (where the asterisk denotes an excited state), and that these excitations decay to a $3p^63d^{n-1}+e^-$ state, thereby resonantly enhancing the direct photoemission process ($3p^63d^n \rightarrow 3p^63d^{n-1}+e^-$). In atomic systems, the multiplet splitting of the $[3p^53d^{n+1}]^*$ excited-state configuration successfully explains the asymmetry, the width, and the rich fine structure in the photoabsorption measurements. In the absorption spectra from the solid transition metals, much of the fine structure is washed out because the itinerant *d* electrons screen the 3*p*-3*d* interaction, thereby reducing the magnitude of the multiplet splittings. However, the main features of the absorption spectra can still be interpreted within an atomic model.[25] In the transition-metal oxides, the 3*d* electrons are more localized than in the corresponding metals, and hence the 3*p* absorption spectra from the oxides exhibit more distinct multiplet features.

Figure 1 shows the total photoelectron yield (TY) measured across the Fe 3*p* threshold from each of the iron oxide single crystals and from an atomically clean polycrystalline Fe foil that was sputter cleaned *in situ*. The total yield measurement, which mirrors the photoabsorption profile, clearly illustrates the resonant behavior around the 3*p* threshold. We observe that the onset of the resonance depends on the oxidation state of the cations and correlates with the Fe 3*p* binding energies determined by XPS,[8,10] which are denoted by the arrows in Fig. 1.

Each of the TY profiles contain features that can be attributed to the different multiplets of the $[3p^53d^{n+1}]^*$ in-

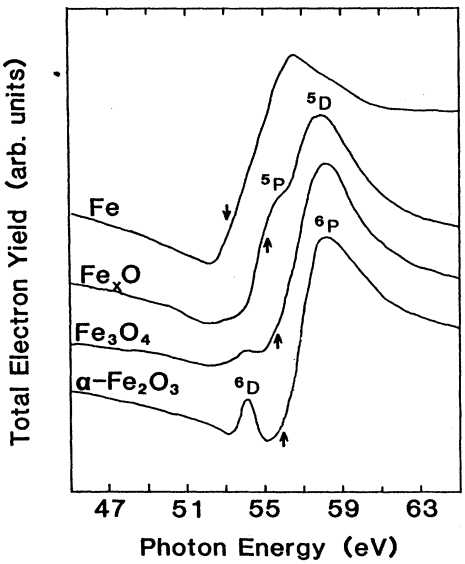

FIG. 1. Total photoelectron yield across the Fe 3*p* excitation threshold measured from a clean Fe foil and from cleaved iron oxide single crystals. Fe_xO contains primarily Fe^{2+} cations, α-Fe_2O_3 contains Fe^{3+} cations, and Fe_3O_4 has both Fe^{3+} and Fe^{2+} cations in a ratio of 2:1. The arrows indicate the location of the Fe 3*p* binding energy for each compound as measured by XPS (Refs. 8 and 10).

termediate states. In α-Fe_2O_3, the Fe^{3+} cations are in a $3p^63d^5$ (^6S) ground-state configuration [analogous to atomic Mn (Ref. 24)]. Of the many possible multiplets for the $[3p^53d^6]^*$ excited state[26] resulting from optical absorption, only the strongest ^6P and ^6D states are visible in the TY spectrum. The main asymmetric resonant profile is associated with the ^6P multiplet, while the symmetric peak at lower photon energy is due to the ^6D multiplet, which is forbidden from decaying into the continua by an angular momentum selection rule.[21] In Fe_xO, the Fe^{2+} cations are in a $3p^63d^6$ (^5D) ground-state configuration [analogous to atomic Fe (Ref. 23)]; the TY spectrum is dominated by features from $3p^63d^6 \rightarrow [3p^53d^7]^*$ ^5D and ^5P excitations. Fe_3O_4 contains both Fe^{3+} and Fe^{2+} cations in a ratio of 2:1, and the TY measurement exhibits a profile that is characteristic of both valence states. As noted previously,[23,27] the photoabsorption from metallic iron does not show any multiplet structure and exhibits only the strong asymmetric resonance profile.

IV. VALENCE-BAND PHOTOEMISSION

The valence band in each of the iron oxides contains overlapping and hybridized Fe $3d$ and O $2p$ states, which are difficult to deconvolute in the photoemission spectra. In this paper we use the resonant photoemission yield across the Fe $3p$ threshold, illustrated in Sec. III, as a means of isolating the Fe $3d$-derived states from the unhybridized O $2p$ states.

In the light transition-metal oxides ($Z < 24$), the onset for the $3p \rightarrow 3d$ resonance is delayed (i.e., occurs at higher photon energy than the $3p \rightarrow 3d$ optical absorption edge), and it has been suggested that interatomic direct recombination in these materials causes both the cation $3d$ and the O $2p$ states to resonate.[28] On the contrary, the $3p \rightarrow 3d$ excitations in the iron oxides and other heavy transition-metal oxides ($Z > 24$) are believed to be quite localized and involve only the $3d$-derived states. Therefore, the difference between valence band EDC's measured just above and below the resonance should eliminate the nonresonating O $2p$ contribution. The resulting difference spectrum reflects the distribution of $3d$-derived final states, which may be either purely Fe $3d$ states or Fe $3d$-derived states that are hybridized with neighboring oxygen ligands. This method of separating the $3d$-derived features in the valence band of transition-metal compounds was initially suggested by Fujimori *et al.*[2,6,29]

In the remainder of this section, we present measurements of the energy distribution of the Fe $3d$-derived photoemission final states in each of the cleaved iron oxide single crystals as determined by the difference method. Constant-initial-state (CIS) spectra are also presented, which help to distinguish the $3d^{n-1}$ from the $3d^nL$ photoemission final states.[2,6,30–32]

A. $Fe_xO(100)$

Fe_xO crystallizes in the fcc rock-salt structure with Fe^{2+} cations located in the octahedral interstices of the O^{2-} anion lattice; the small number of Fe^{3+} cations associated with the deviation from FeO stoichiometry are situated in tetrahedral sites.[33] An isolated Fe^{2+} cation has a high-spin $3d^6(t_{2g}^4e_g^2)$ ground-state configuration with $^5T_{2g}$ symmetry.

Angle-integrated EDC's measured from cleaved $Fe_xO(100)$ with photon energies between $48 \leq h\nu \leq 65$ eV are shown in Fig. 2. In each spectrum, the upper edge of the valence band is observed to coincide with the Fermi level. Significant changes are visible in the shape of the valence-band spectra as the $3d$ states resonate above the $3p$ excitation threshold. Most noticeable are the increases in emission at binding energy locations $\simeq 1$, 4, and 11 eV. The arrows in Fig. 2 show the constant kinetic energy positions where the $M_{23}M_{45}M_{45}$ super-Coster-Kronig Auger transition should appear; no discernible intensity is visible. Figure 3 shows the difference between EDC's taken at 57 and 54 eV, corresponding to above and below resonance (see Fig. 1); an integral inelastic background was removed from each spectrum prior to taking the difference. The $3d$-derived states measured by the difference spectrum extend to about 16 eV below the Fermi level, in agreement with Fujimori's result,[2] and exhibit maxima at 1.2, 4.1, 6.9, and 11.0 eV.

A simple crystal-field-theory description of the $3d^5$ final states in the photoemission spectra from Fe_xO was first suggested by Eastman and Freeouf.[1] The $3d^5$ final states with allowed symmetry were identified as $^6A_{1g}$, $^4A_{1g}$, ^4E_g, $^4T_{1g}$, and $^4T_{2g}$, and they were all estimated to occur within 6 eV of the Fermi level. Later, Bagus *et al.*[13] considered configuration-interaction wave functions and used improved estimates for the crystal-field parameters to conclude that the width of the Fe $3d$ final states should extend to about 10 eV below the Fermi lev-

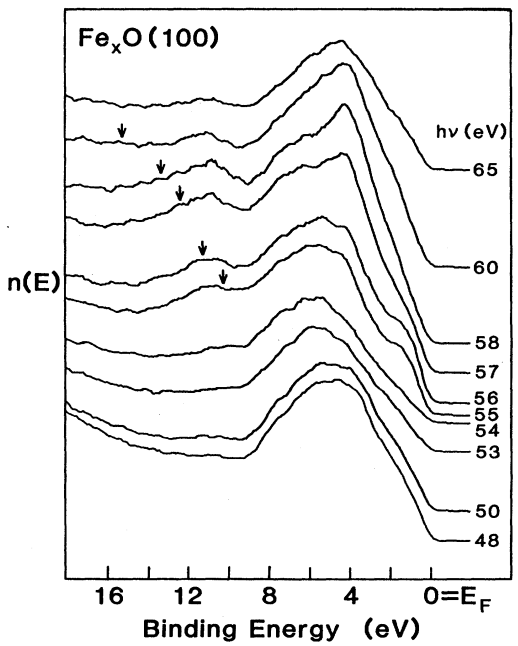

FIG. 2. Angle-integrated EDC's measured from cleaved $Fe_xO(100)$. The $M_{23}M_{45}M_{45}$ Auger transition should appear at the constant kinetic energy location indicated by the arrows.

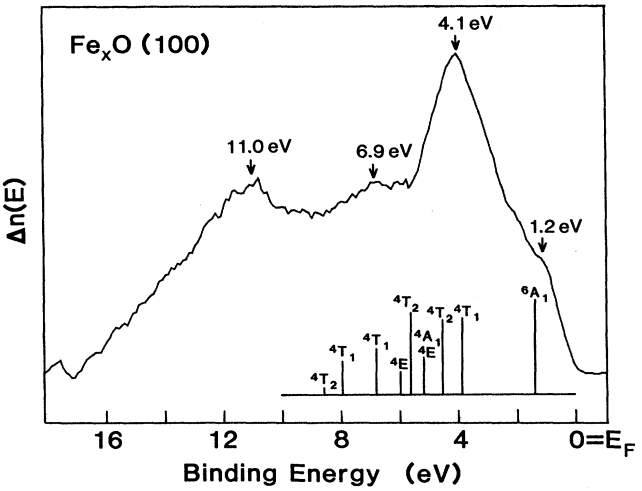

FIG. 3. Fe 3*d*-derived final states in Fe$_x$O(100) determined by the difference between EDC's measured at 57 and 54 eV; integral inelastic backgrounds have been subtracted from the EDC's prior to taking differences. The vertical lines show the $3d^5$ final-state positions predicted in Ref. 13.

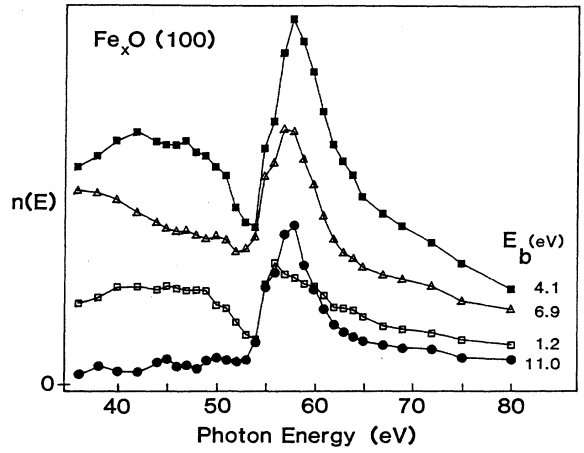

FIG. 4. CIS spectra from Fe$_x$O(100) across the Fe 3*p* excitation threshold measured at the binding energies (E_b) corresponding to the maxima in the 3*d*-derived states shown in Fig. 3. The intensities are plotted on the same $n(E)$ scale.

el. As shown by the relative positions and intensities of their calculated $3d^5$ final states[13] in Fig. 3, the crystal-field analysis roughly explains some of the main features near the top of the valence-band spectrum but cannot account for any of the 3*d* intensity extending 16 eV below the Fermi level.

The additional 3*d*-derived intensity between 9 and 16 eV that is left unaccounted for by crystal-field theory can be explained by covalency effects between the Fe^{2+} cations and the surrounding O^{2-} ligands. This interpretation has emerged from recent CI cluster calculations for an isolated transition-metal cation and surrounding ligands which allow for the possibility of ligand-to-metal charge transfer in both the initial and final state.[6,30] The calculations, first done for NiO,[30] suggest that the final states near the Fermi level are primarily $3d^nL$-like, while the $3d^{n-1}$ states are concentrated at higher binding energies (at the so-called satellite position). This same assignment has been postulated by Fujimori *et al.*[2] to explain the 16-eV-wide distribution of Fe 3*d*-derived final states in Fe$_x$O.

Constant-initial-state (CIS) spectra measured across the 3*p* excitation threshold can be used to identify hybridized cation-ligand states in the valence band. In the CIS spectra, Fano-like resonances are expected from $3d^{n-1}$ states, whereas antiresonant profiles should be observed from the $3d^nL$ states associated with ligand-to-metal charge transfer.[30–32] Our CIS measurements from cleaved Fe$_x$O are shown in Fig. 4 for the binding energy positions corresponding to the maxima in Fig. 2; they are in close agreement with previous CIS spectra reported from reduced sintered Fe$_x$O samples.[2] Each of the CIS spectra exhibit the same multiplet features discussed in Sec. III, namely the ^5P-derived shoulder at 55 eV and the ^5D-derived maximum at 57 eV. It is evident that the 1.2 eV feature has an antiresonant profile, and hence the top of the valence-band spectrum is assigned to $3d^6L$ final states. Similarly, the 11.0-eV feature resonates with a Fano-like profile which indicates that $3d^5$ final states dominate this region of the valence-band spectrum. The CIS profiles at 4.1 and 6.9 eV show both antiresonant and resonant behavior, suggesting that $3d^5$ and $3d^6L$ states overlap in this energy range. However, care must be used in interpreting CIS profiles for binding energies between 2 and 8 eV since they include intensity from the unhybridized O 2*p* states, which have a decreasing cross section with increasing photon energy.

B. α-Fe_2O_3 ($10\bar{1}2$)

α-Fe_2O_3 has the corundum (trigonal) lattice in which each Fe^{3+} cation is surrounded by a distorted octahedron of O^{2-} ions;[33] the distortion is small so that the local structural environment of each cation is essentially the same as in Fe$_x$O. The ground-state configuration of the Fe^{3+} cation is $3d^5(t_{2g}^3e_g^2)$ with $^6A_{1g}$ symmetry.

Figure 5 shows EDC's measured from cleaved α-$Fe_2O_3(10\bar{1}2)$ for $48 \leq h\nu \leq 65$ eV. Due to the insulating nature of α-Fe_2O_3, the Fermi level lies in the bulk band gap about 1.3 eV above the upper edge of the valence band. At photon energies above the 3*p* threshold, the largest change in the EDC's is observed near the satellite position ($\simeq$13 eV), where the resonant enhancement is much larger than was seen in Fe$_x$O (Fig. 2); there appears to be no contribution from the $M_{23}M_{45}M_{45}$ Auger emission, whose location is indicated by the arrows in Fig. 5. Figure 6 shows the distribution of the 3*d*-derived final states determined from the difference between EDC's at 58 and 55 eV, corresponding to above and below the resonance in Fig. 1. A three-peaked structure extending 18 eV below the Fermi level is observed, with maxima at approximately 3.1, 6.2, and 12.9 eV. Our results concur with the EDC's reported by Fujimori *et al.*[6] from re-

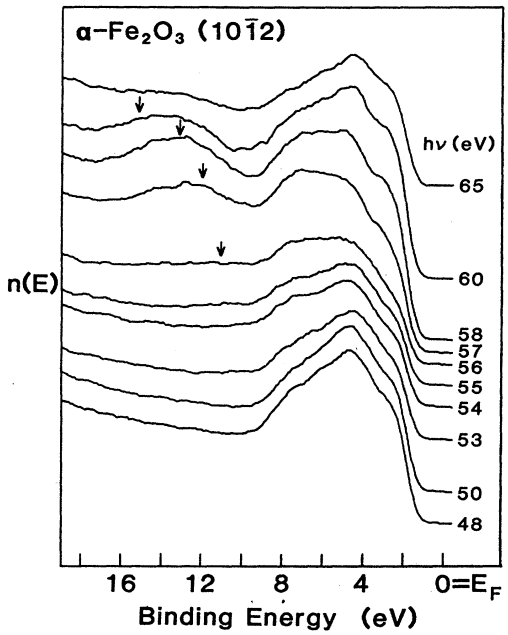

FIG. 5. Angle-integrated EDC's measured from cleaved α-$Fe_2O_3(10\bar{1}2)$. The predicted location of $M_{23}M_{45}M_{45}$ Auger emission is shown by the arrows.

duced sintered α-Fe_2O_3 samples, but the spectral features measured with higher energy resolution from our cleaved α-Fe_2O_3 single crystal are more distinct.

The results from Fujimori's CI calculation for a $(FeO_6)^{9-}$ cluster[6] are compared to the experimental distribution of the $3d$-derived final states in Fig. 6. The vertical lines show the calculated positions and relative intensities for both $3d^4$ and $3d^5L$ photoemission final states. The CI cluster model, which includes covalency in both the initial (ground) and final states, successfully explains the origin of the 18-eV-wide spectrum; $3d^5L$ states are primarily concentrated between 0 and 9 eV, while the $3d^4$ states comprise the 9–18-eV region. The CIS profiles shown in Fig. 7 test the validity of these final-state assignments. The 12.9-eV feature shows only a resonance, while the profiles for binding energies of 7.8, 5.3, and 3.1 eV exhibit an antiresonant dip preceeding the resonance which becomes more pronounced with decreasing binding energy. These results are consistent with the predicted assignments of $3d^4$ and $3d^5L$ final states. However, we observe that our CIS spectra measured from cleaved single crystal α-Fe_2O_3 at binding energies near E_F still exhibit a resonant component, suggesting that the energy separation between the $3d^4$ and $3d^5L$ final states in a α-Fe_2O_3 is somewhat smaller than that reported by Fujimori *et al.*[6]

C. Fe_3O_4(110)

Fe_3O_4 is a mixed-valence compound with the cubic inverse spinel structure containing Fe^{3+} and Fe^{2+} cations in a ratio of 2:1. The structure is composed of an fcc lattice of O^{2-} anions with the Fe^{2+} and half of the Fe^{3+} cations located in octahedral interstitial sites and the remaining Fe^{3+} cations situated in tetrahedral sites;[33] a convenient notation is $[Fe^{3+}]_{tet}[Fe^{3+}Fe^{2+}]_{oct}O^{2-}{}_4$. At room temperature, the Fe^{3+} and Fe^{2+} cations randomly occupy the octahedral sites with a hopping frequency on the order of 10^{-11} sec.[34] Since the time scale in the photoemission experiment is on the order of 10^{-15} sec, which is much faster than the hopping frequency, the ground-state cation configurations can be viewed as

$$3d^6(t_{2g}^4e_g^2)^5T_{2g} \quad \text{for } Fe^{2+}{}_{oct},$$

$$3d^5(t_{2g}^3e_g^2)^6A_{1g} \quad \text{for } Fe^{3+}{}_{oct},$$

$$3d^5(e_g^2t_{2g}^3)^6A_{1g} \quad \text{for } Fe^{3+}{}_{tet}.$$

The final-state symmetries and intensities for the multiplet and crystal-field-split Fe^{3+} cations are the same for both the octahedral and tetrahedral coordination,[14] but their relative energies are different.

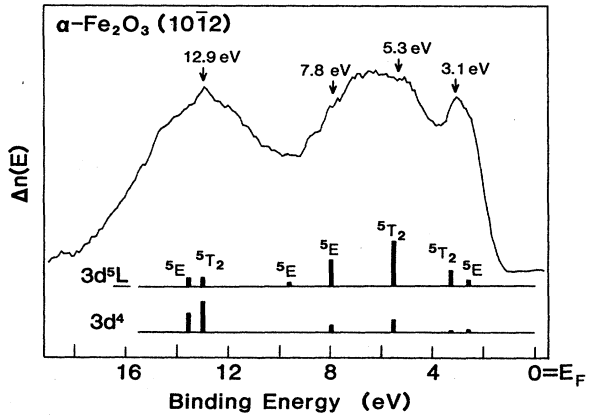

FIG. 6. Fe $3d$-derived final states in α-$Fe_2O_3(10\bar{1}2)$ determined by the difference between EDC's measured at 58 and 55 eV; integral inelastic backgrounds have been subtracted. The $3d^4$ and $3d^5L$ final state positions and relative intensities predicted in Ref. 6 are indicated by vertical lines.

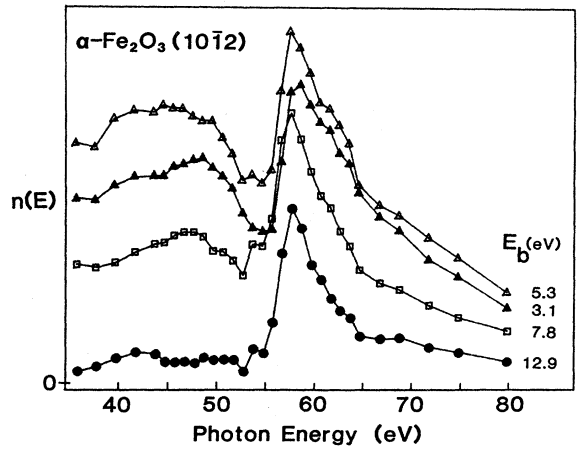

FIG. 7. CIS spectra from α-$Fe_2O_3(10\bar{1}2)$ across the Fe $3p$ excitation threshold measured at the binding energy locations shown in Fig. 6.

Figure 8 shows angle-integrated EDC's measured from $Fe_3O_4(110)$ over the same photon energy range as shown in Figs. 2 and 5 for Fe_xO and α-Fe_2O_3. Many of the same features above the $3p$ excitation threshold that were associated with Fe^{2+} cations in Fe_xO and Fe^{3+} cations in α-Fe_2O_3 are visible in the Fe_3O_4 spectra. The most obvious feature is the 1.2-eV peak characteristic of the Fe^{2+} valence state. The origin of the broad satellite emission centered at 12 eV can be understood by recognizing that the $3d^{n-1}$ final states are centered around 11 eV in Fe_xO (Fig. 2) and around 12.9 eV in α-Fe_2O_3 (Fig. 5); since Fe_3O_4 contains both Fe^{2+} and Fe^{3+} cations, satellite emission occurs at both positions.

The energy location of the satellite emission in Fig. 8 appears to shift for photon energies between $56 \leq h\nu \leq 60$ eV. This shift appears similar to that predicted for an $M_{23}M_{45}M_{45}$ Auger emission peak,[5] which is expected to disperse at the constant kinetic energy shown by the arrows. However, there is an alternative explanation for the apparent shift which we believe is more probable, since the Auger emission peak is not seen for either Fe_xO or α-Fe_2O_3. Referring to the CIS spectra measured from Fe_xO and α-Fe_2O_3 at binding energies of 11.0 eV (Fig. 4) and 12.9 eV (Fig. 7), it is evident that the resonant profiles for the satellite emission associated with either Fe^{2+} and Fe^{3+} valence states are quite different. Specifically, the resonant threshold occurs at a lower photon energy for Fe^{2+} cations than for Fe^{3+} cations. As a result, the satellite in Fig. 8 is concentrated near 11 eV for photon energies below the Fe^{3+} threshold ($h\nu < 57$ eV), and its maximum shifts towards 12.9 eV with increasing photon energy as the Fe^{3+}-derived emission becomes dominant. For $h\nu = 60$ eV, very little intensity is observable at the predicted $M_{23}M_{45}M_{45}$ location, which supports this satellite interpretation.

Estimates of the Fe $3d$-derived final states in Fe_3O_4 are shown in Fig. 9 in terms of three difference spectra. The 58–54-eV spectrum corresponds to the difference between EDC's measured just above and below the resonance in Fe_3O_4 shown in Fig. 1. Consequently, it reflects the energy distribution of the $3d$-derived states from both the Fe^{2+} and Fe^{3+} cations. By taking a 57–54-eV difference spectrum, the final states from the Fe^{2+} cations tend to be emphasized since most of the resonance from Fe^{2+} cations occurs within this energy range (as shown for Fe_xO in Fig. 1). Likewise, a 58–55-eV difference spectrum highlights the Fe^{3+}-related features, although some intensity from the Fe^{2+} cations is of course included. The arrows shown in Fig. 9 correspond to the maxima in the Fe^{2+} and Fe^{3+} $3d$-derived photoemission features measured from Fe_xO (Fig. 3) and α-Fe_2O_3 (Fig. 6), respectively. The same Fe^{2+}- and Fe^{3+}-derived features are visible in the difference spectra measured from Fe_3O_4.

The CIS spectra in Fig. 10 corresponding to various binding energies throughout the valence band of Fe_3O_4 are remarkably similar to those from Fe_xO (Fig. 4) and α-Fe_2O_3 (Fig. 7); final states between 0 and 10 eV exhibit antiresonant $3d^nL$-like profiles, and states between 10 and 18 eV show $3d^{n-1}$ resonances.

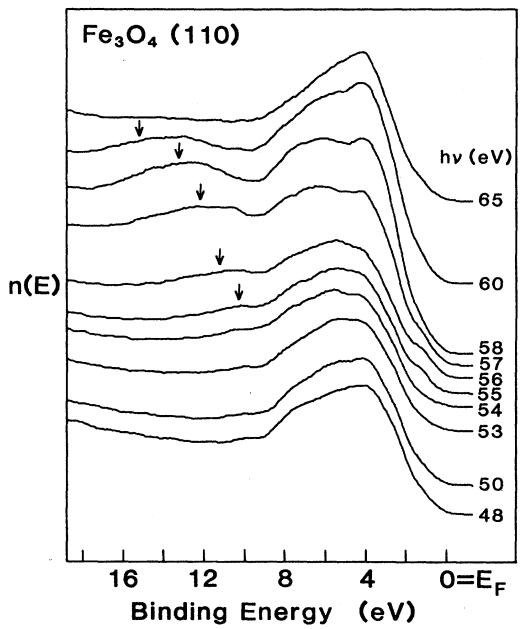

FIG. 8. Angle-integrated EDC's measured from cleaved $Fe_3O_4(110)$. The predicted location of the $M_{23}M_{45}M_{45}$ Auger emission is shown by the arrows.

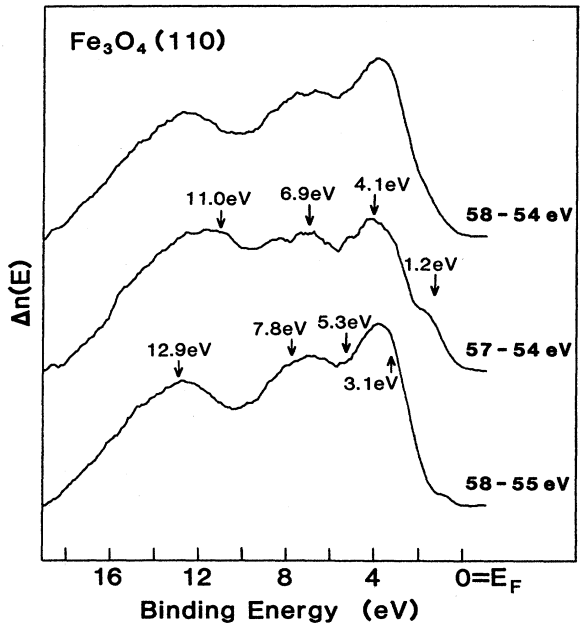

FIG. 9. Fe $3d$-derived final states in $Fe_3O_4(110)$ determined by differences between EDC's measured at 58 and 54 eV, at 57 and 54 eV (emphasizing Fe^{2+} features), and at 58 and 55 eV (emphasizing Fe^{3+} features). Integral inelastic backgrounds were subtracted from each spectrum prior to taking differences.

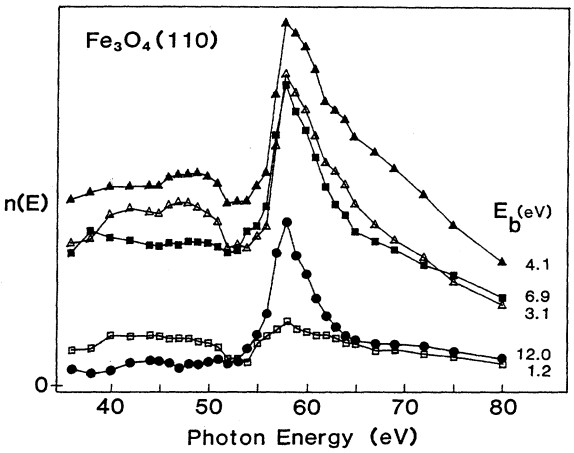

FIG. 10. CIS spectra from $Fe_3O_4(110)$ across the Fe $3p$ excitation threshold measured at the binding energy locations corresponding to both the Fe^{2+} and the Fe^{3+} derived features shown in Fig. 9.

V. DISCUSSION

In many previous photoemission studies of iron oxides, measurements of the complex valence band were further confounded by nonstoichiometric and highly defective samples. We have performed resonant photoemission measurements on cleaved stoichiometric single crytals of Fe_xO, Fe_3O_4, and α-Fe_2O_3 using the same spectrometer, and thus we have been able to identify the subtle differences that exist in the valence-band features associated with each cation valence state. We conclude that the main characteristics that distinguish Fe^{2+} from Fe^{3+} emission are (i) the presence of a Fe^{2+} $3d$-derived peak within 1.5 eV of the Fermi level and (ii) a satellite maximum for Fe^{2+} located at a binding energy (11.0 eV) about 2 eV lower than for Fe^{3+} (12.9 eV).

The valence-band region in each oxide extends about 18 eV below the Fermi level; this observation is most prominent at photon energies above the $3p \rightarrow 3d$ excitation threshold. A plausible explanation for the large spectral width is offered by the results of Fujimori's CI cluster calculations.[6,30] Within the cluster model, the $3d$ electrons are assumed to be localized at the cation sites but are allowed to have covalent interactions with neighboring O^{2-} ligands. The cation-ligand hybridization leads to the existence of both $3d^{n-1}$ and $3d^nL$ final-state features which are spread over an 18-eV-wide energy range. The shapes of the resonant profiles in our CIS data give credence to this interpretation as discussed in the previous section. Since primarily $3d^nL$ final states are located near the Fermi level in the photoemission spectra from each of the iron oxides, we classify them as charge-transfer rather than Mott-Hubbard insulators.

The resonant-photoemission-difference method utilized in Sec. IV emphasizes the Fe $3d$-derived valence states; these include unhybridized cation $3d$ states as well as states created by cation-ligand hybridization. The distribution of the unhybridized O $2p$ states is removed from the difference spectra and hence the question still remains as to the exact location of the O $2p$ region. Figure 11 shows EDC's from each of the iron oxides measured at a photon energy of 30 eV, where the Fe $3d$ ionization cross section is small relative to that for O $2p$ emission. Based on the spectral shapes, we conclude that the O $2p$ emission exhibits a single broad maximum centered between about 2 and 8 eV; the peak shape is essentially identical in each of the iron oxide phases. These results are in agreement with previous studies.[1,2,4,6,12,13]

The resonant-photoemission phenomenon can be viewed as a localized probe of the $3d$-derived valence states because the $3p \rightarrow 3d$ excitations are intra-atomic in nature. Accordingly, the onset of the resonance is observed to depend on the oxidation state of the Fe cations. This fact enables one to interpret the photoemission spectra from the mixed-valence compound Fe_3O_4. An Fe_3O_4 difference spectrum taken between EDC's at photon energies above and below resonance (i.e., 58–54 eV) will contain three separate contributions: the $3d$-derived states associated with $Fe^{2+}{}_{oct}$, $Fe^{3+}{}_{oct}$, and $Fe^{3+}{}_{tet}$ cations. By taking appropriate difference spectra (see Fig. 9), either the Fe^{2+} or Fe^{3+} contributions can be accentuated. Comparing Fig. 9 with Figs. 3 and 6, it is evident that most of the same $3d$-derived features associated with Fe^{2+} cations in Fe_xO and Fe^{3+} cations in α-Fe_2O_3 are also visible in the Fe_3O_4 spectra. This result lends credence to an interpretation of the $3d$-derived features in terms of covalent interactions between each isolated Fe cation and its neighboring O^{2-} ligands in octahedral or tetrahedral environments. A complete theoretical determination of the valence states in Fe_3O_4 which includes hybridization between the cation $3d$ and ligand $2p$ orbitals would be very complex and has not yet been performed. However, the CIS measurements indicate that

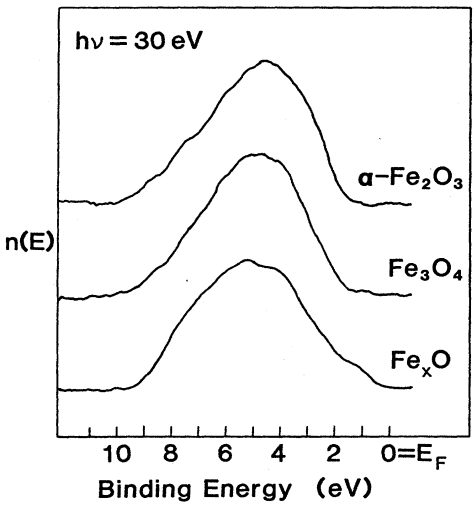

FIG. 11. EDC's measured from cleaved iron oxides at $h\nu = 30$ eV, which emphasizes the O $2p$ emission. An inelastic background has been removed from each spectrum.

Fe_3O_4 can be regarded as a charge-transfer insulator, similar to Fe_xO and α-Fe_2O_3.

VI. SUMMARY

Results of resonant photoemission measurements of the Fe 3*d*-derived valence states in cleaved single crystals of Fe_xO, Fe_3O_4, and α-Fe_2O_3 have been reported. Due to the localized nature of the Fe 3*p* excitations involved in the resonant-photoemission mechanism, the origin of the valence-band features has been interpreted in terms of an isolated iron cation situated in either an octahedral or tetrahedral environment of O^{2-} ligands. This same cluster model is the basis for the recent configuration-interaction calculations for α-Fe_2O_3 by Fujimori *et al.* The experimental results from cleaved α-Fe_2O_3 agree directly with the cluster calculations of photoemission final states, and they confirm the need to consider ligand-to-metal charge-transfer effects in order to understand valence-band photoemission spectra. The more complex calculations required for Fe_xO and Fe_3O_4 have yet to be performed, so we have nothing with which to compare our measurements. But the CIS spectra presented in Sec. IV reveal that hybridization between cation 3*d* and ligand 2*p* orbitals must be an essential feature of their electronic structures as well.

ACKNOWLEDGMENTS

We wish to thank C. R. Brundle and A. Revcolevschi for Fe_xO, D. J. Buttrey for Fe_3O_4, and J. P. Remeika for α-Fe_2O_3 single crystals. We are also grateful to K. E. Smith for technical help and many useful discussions. The support of the NSLS staff, especially R. F. Garrett, C. Hirschmugl, and G. P. Williams, was greatly appreciated. This work was partially supported by NSF (National Science Foundation) Solid State Chemistry Grant No. DMR-87-11423. Research was performed at the National Synchrotron Light Source (NSLS), Brookhaven National Laboratory, which is supported by (Department of Energy) DOE, Division of Materials Sciences and Division of Chemical Sciences, Contract No. DE-AC02-76CH00016.

---

*Present address: Laboratory for Surface Science & Technology and Department of Physics & Astronomy, University of Maine, Orono, ME 04469.

[1]D. E. Eastman and J. L. Freeouf, Phys. Rev. Lett. **34**, 395 (1975).

[2]A. Fujimori, N. Kimizuka, M. Taniguchi, and S. Suga, Phys. Rev. B **36**, 6691 (1987).

[3]S. F. Alvarado, W. Eib, F. Meier, D. T. Pierce, K. Sattler, H. C. Siegmann, and J. P. Remeika, Phys. Rev. Lett. **34**, 319 (1975).

[4]S. F. Alvarado, M. Erbudak, and P. Munz, Phys. Rev. B **14**, 2740 (1976).

[5]K. Siratori, S. Suga, M. Taniguchi, K. Soda, S. Kimura, and Y. Yanase, J. Phys. Soc. Jpn. **55**, 690 (1986).

[6]A. Fujimori, M. Saeki, N. Kimizuka, M. Taniguchi, and S. Suga, Phys. Rev. B **34**, 7318 (1986).

[7]N. Beatham, A. F. Orchard, and G. Thornton, J. Phys. Chem. Solids **42**, 1051 (1981).

[8]N. S. McIntyre and D. G. Zetaruk, Anal. Chem. **49**, 1521 (1977).

[9]S. Vasudevan, M. S. Hedge, and C. N. R. Rao, J. Solid State Chem. **29**, 253 (1979).

[10]C. R. Brundle, T. J. Chuang, and K. Wandelt, Surf. Sci. **68**, 459 (1977).

[11]C. R. Brundle, Surf. Sci. **66**, 581 (1977).

[12]G. Grenet, Y. Jugnet, T. M. Duc, and M. Kibler, J. Chem. Phys. **72**, 218 (1980); **74**, 2163 (1981).

[13]P. S. Bagus, C. R. Brundle, T. J. Chuang, and K. Wandelt, Phys. Rev. Lett. **39**, 1229 (1977).

[14]P. S. Bagus, J. L. Freeouf, and D. E. Eastman, Phys. Rev. B **15**, 3661 (1977).

[15]S. H. Chou, J. Guo, and D. E. Ellis, Phys. Rev. B **34**, 12 (1986).

[16]A. Yanase and K. Siratori, J. Phys. Soc. Jpn. **53**, 312 (1984).

[17]J. Zaanen, G. A. Sawatzky, and J. W. Allen, Phys. Rev. Lett. **55**, 418 (1985); J. Magn. Mater. **54-57**, 607 (1986).

[18]J. Zaanen and G. A. Sawatzky, Can. J. Phys. **65**, 1262 (1987).

[19]L. S. Darken and R. W. Gurry, J. Am. Chem. Soc. **67**, 1398 (1945); **68**, 798 (1946).

[20]J. Stöhr, R. Jaeger, J. Feldhaus, S. Brennan, D. Norman, and G. Apai, Appl. Opt. **19**, 3911 (1980).

[21]L. C. Davis, J. Appl. Phys. **59**, R25 (1986).

[22]R. Bruhn, B. Sonntag, and H. W. Wolff, J. Phys. B **12**, 203 (1979).

[23]E. Schmidt, H. Schroder, B. Sonntag, H. Voss, and H. E. Wetzel, J. Phys. B **16**, 2961 (1983).

[24]R. Bruhn, E. Schmidt, H. Schroder, and B. Sonntag, Phys. Lett. **90A**, 41 (1982); E. Schmidt, H. Schroder, B. Sonntag, H. Voss, and H. E. Wetzel, J. Phys. B **18**, 79 (1985).

[25]L. C. Davis and L. A. Feldkamp, Solid State Commun. **19**, 413 (1976).

[26]L. C. Davis and L. A. Feldkamp, Phys. Rev. A **17**, 2012 (1978).

[27]B. Sonntag, R. Haensel, and C. Kunz, Solid State Commun. **7**, 597 (1969).

[28]K. E. Smith and V. E. Henrich, Phys. Rev. B **38**, 9571 (1988).

[29]M. Taniguchi, A. Fujimori, M. Fujisawa, T. Mori, I. Souma, and Y. Oka, Solid State Commun. **62**, 431 (1987); L. Ley, M. Taniguchi, J. Ghijsen, R. L. Johnson, and A. Fujimori, Phys. Rev. B **35**, 2839 (1987).

[30]A. Fujimori, F. Minami, and S. Sugano, Phys. Rev. B **29**, 5225 (1984); A. Fujimori and F. Minami, **30**, 957 (1984).

[31]L. C. Davis, Phys. Rev. B **25**, 2912 (1982).

[32]G. van der Laan, Solid State Commun. **42**, 165 (1982).

[33]J. B. Goodenough, in *Metallic Oxides,* edited by H. Reiss (Pergamon, New York, 1972) [Prog. Solid State Chem. **5**, 145 (1972)].

[34]B. Balko ad G. R. Hoy, Physica B+C **86-88B**, 953 (1977).